RSC Advances




ROYAL SOCIETY OF CHEMISTRY

www.rsc.org/advances

Journal Name

RSCPublishing

ARTICLE

# A high-performance n-butanol gas sensor based on ZnO nanoparticles synthesized by a low-temperature solvothermal route

Cite this: DOI: 10.1039/x0xx00000x

Received 00th January 2012,
Accepted 00th January 2012

DOI: 10.1039/x0xx00000x

www.rsc.org/

Xu Liu,[a] Nan Chen,[a] Xinxin Xing,[a] Yuxiu Li,[a] Xuechun Xiao,[a,b] Yude Wang,*[a,b] and Igor Djerdj*[c]

ZnO nanoparticles with high crystallinity and several nanometers in size were synthesized by a low-temperature solvothermal route from zinc acetate dihydrate ($Zn(CH_3COO)_2 \cdot 2H_2O$), potassium hydroxide (KOH) and methanol ($CH_3OH$). The structural and the morphological characterizations of ZnO nanoparticles were performed by X-ray powder diffraction (XRD), transmission electron microscopy (TEM), X-ray photoelectron spectroscopy (XPS) and $N_2$-sorption isotherm. The obtained nanoparticles are highly crystalline wurtzite-type ZnO with uniform near-sphere shape with an average particle size estimated to 8.4±1.3 nm. Such a small particle size and slight agglomeration are attributed to the use of methanol which acts as both solvent and inhibitor of growth and agglomeration. The as-synthesized ZnO nanoparticles were directly used as a gas sensing material toward n-butanol gas. Such designed sensor device exhibits several advantages such as high and fast response, short recovery time, and good stability toward n-butanol gas. At the optimal operating temperature (320 ºC), its gas response toward 500 ppm n-butanol is 805 and the response and recovery time are 22 and 6 seconds, respectively.

## 1. Introduction

Volatile organic compounds (VOCs) are a group of chemical compounds that easily evaporate at room temperature.[1] They are not only harmful for the environment but also considered seriously affecting human's health and security.[2] For instance, n-butanol, an important solvent, organic synthesis raw material and extracting agent, is widely used in laboratory and factory. Such agent is a stimulating and narcotic liquid. Exposing to n-butanol vapour could cause several symptoms such as headache, dizzy, drowsiness, dermatitis and discomfort of eyes, nose as well as throat.[3] Many countries' specified threshold limit value of n-butanol in the work place is only 152-304 $mg/m^3$ such as 200 $mg/m^3$ for China, 304 $mg/m^3$ for Occupational Safety and Health Administration (OSHA), 152 $mg/m^3$ for the American Conference of Governmental Industrial Hygienists (ACGIH), and so on. Moreover, n-butanol is also inflammable. Air mixture which contains of 1.45 % to 11.25 % n-butanol by volume may cause explode or flash fire at a temperature higher than its flash point (35 ºC). Its product of combustion contains CO and $CO_2$ which are suffocating gases. Thus high performance sensors to monitor n-butanol for laboratories and factories are needed. Compared with traditional method such as chromatography,[3] semiconductor metal oxide based gas sensor is thought to be the most promising miniaturized gas-sensing device owning to its high sensitivity, fast response, low cost and small size.

As one of the most versatile semiconductor material, the wurtzite-type ZnO with a wide band gap energy (3.37 eV) and very large excitation binding energy (60 meV) at room temperature[4] plays an important role in various technological domains such as solar cells,[5] spintronic devices,[6] photodetectors,[7] light emitting diodes,[8] and nanolasers[9] owing to its combination of optical and electrical properties. ZnO is also an excellent substance used for detection of VOCs due to its low cost, high sensitivity and quick gas recovery.[10,11] It is known that the morphology has a great influence on the gas sensing properties of materials,[12] and the composite of noble metal[13] or other metal oxide[11] can significantly increase their gas sensing properties. Up to now, lot of different morphological ZnO and ZnO based composite have been prepared and used for detecting n-butanol such as ZnO nanoflakes,[14] ZnO nanowires,[15] ZnO microflowers,[16] Au-functionalized porous ZnO microsheets,[17] ZnO-decorated α-

$Fe_2O_3$,[18] and so on. Though they get a better gas response toward n-butanol than other metal oxide semiconductor (e.g., $SnO_2$ nanospheres,[19] α-$Fe_2O_3$ hollow spindles,[20] $ZnSnO_3$ nanocubes,[21] $WO_3$ nanoflowers,[22] NiO hollow spheres,[23] and so on), the performances including sensitivity, selectivity, response and recovery time for n-butanol detecting is still un-ideal. The high sensing material for the detection of n-butanol gas is still to be developed. Recent contributions have shown that these performance indexes could be improved by a smaller grain size which will result in higher specific surface area.[16,24] Therefore, the well crystallized ZnO nanoparticles with small grain size ought to have a good gas sensing property.

This paper describes a simple low-temperature solvothermal route to ZnO nanoparticles with high crystallinity for gas sensing purposes. The obtained ZnO nanoparticles were used to fabricate gas sensor which shows a high sensitivity, a good selectivity, a fast response and recovery, a good repeatability and stability toward n-butanol gas. The structure, morphology, chemical state, and specific surface area are also investigated to give a further understanding of related nanocrystals formation and gas sensing mechanisms.

## 2. Experimental

### 2.1. Preparation of ZnO nanoparticles

All the chemical reagents used in the experiments were obtained from commercial sources as guaranteed-grade reagents and used without further purification.

ZnO nanoparticles were prepared by a simple low-temperature solvothermal method. In a typical synthetic experiment, 0.5817 g of $Zn(CH_3COO)_2{\cdot}2H_2O$ and 0.2700 g of KOH were dissolved into 25 mL and 15 mL methanol to get transparent solutions, respectively. Later, the solution of potassium hydroxide was poured into zinc acetate solution to form a white suspension. The pH of the suspension is measured to be 8. After magnetically stirring for 20 min, 33 mL of the mixture was transferred into a Teflon-lined stainless steel autoclave with a capacity of 55 mL and reacted under solvothermal conditions at 100 ºC for 4 h. The autoclave was cooled down to room temperature in standard atmosphere. The resulting product was centrifuged, and the white precipitate was thoroughly washed with ethanol and dried at 60 ºC overnight. The reaction yield was estimated to be 81.3%.

### 2.2. Characterization

X-Ray diffraction (XRD, Rigaku D/MAX-3B powder diffractometer) with a copper target and $K_\alpha$ radiation (λ=1.54056 Å) was used for the phase identification, where the diffracted X-ray intensities were recorded as a function of $2\theta$. The sample was scanned from 10° to 90° ($2\theta$) in steps of 0.01°. The transmission electron micrographs (TEM) were obtained with a Zeiss EM 912 Ω instrument at an acceleration voltage of 120 kV, while high-resolution transmission electron microscopy (HRTEM) characterization was done using a Philips CM200-FEG microscope (200 kV, $C_s$=1.35 mm). The samples for TEM were prepared by dispersing the final dry powders in ethanol; this dispersion was then dropped on carbon-copper grids. Nitrogen adsorption isotherm was measured at 77.3 K with a Micromeritics ASAP 2010 automated sorption analyzer. Prior to the measurement, the sample was degassed at 300 °C for 3 h under vacuum. X-ray photoelectron spectroscopy (XPS) was carried out at room temperature in ESCALAB 250 system. During XPS analysis, an Al Kα X-ray beam was adopted as the excitation source and the vacuum pressure of the instrument chamber was $1\times10^{-7}$ Pa as read on the panel. Measured spectra were decomposed into Gaussian components by a least-square fitting method. Bonding energy was calibrated with reference to C1s peak (285.0 eV).

### 2.3. Fabrication and measurement of gas sensor

The test gas sensor system was fabricated according to the literature.[25] At the very beginning, the as-synthesized products were mixed with an appropriate deionized water to form a paste. Afterwards, the paste was coated by a paint pen onto the outside surface of an alumina tube (4 mm in length, 1.2 mm in external diameter, and 0.8 mm in internal diameter) with a pair of Au electrodes at each end connected by platinum wires. The thickness of the gas sensing materials is about 54 μm to uniformly cover the whole Au electrodes to guarantee a good contact.(Fig. S1) Next, the sensors were calcined in air at 400 °C for 2 h and then a Ni-Cr heating wire was inserted in the tube to control the operating temperature via a heating voltage ($V_h$), as shown in Fig. S2. In order to improve the stability and repeatability, the fabricated sensors were aged at 320 ºC for 48 h in air. Finally, the sensors were well connected to bakelite base through platinum wires to perform electrical measurements using a WS-30A system (Weisheng Instruments Co. Zhengzhou, China, as seen in Fig. S2). During the testing process, the desired amounts of target substance were injected into the chamber by a microsyringe after the resistances of all the sensors were stable. The analyte solution was evaporated by a quick evaporator and mixed with air immediately by two installed fans in the chamber (18 L in volume). The gas response $\beta$ was defined as the ratio of the electrical resistance in air ($R_0$) to that in gas ($R_g$). In addition, the response time was defined as the time required for the gas response reaching 90% of the final equilibrium value after a test gas was injected, and the recovery time was the time needed for gas response decreasing its 90% after the gas sensor was exposed in air again.

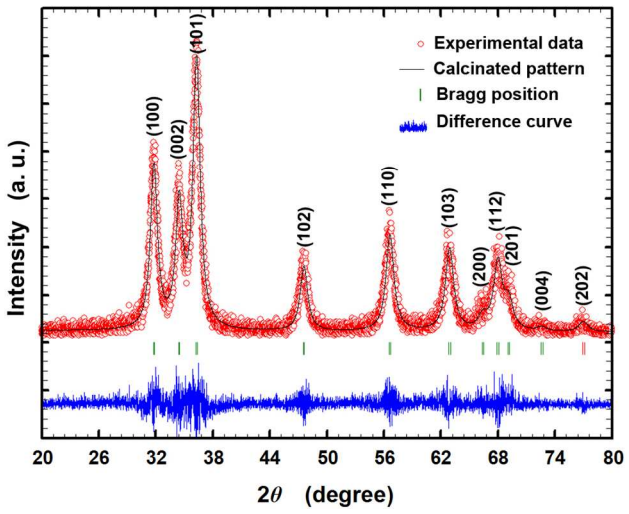


**Fig. 1** Typical Rietveld output plot of as-prepared ZnO nanoparticles. The experimental data is shown in red, the calculated pattern in black, and the difference curve in blue. The short vertical bars in green represent the positions of the Bragg reflections.

## 3. Results and discussion

The structural and microstructural features of as-prepared ZnO nanoparticles were analyzed by the X-ray diffraction (XRD). The initial assignment is further confirmed by the refinement of the diffraction pattern with the Rietveld method. The experimental pattern, together with the calculated pattern obtained from the Rietveld refinement and difference profile thereof are shown in Fig. 1. The difference curve between the calculated and experimental XRD patterns indicates an excellent agreement. The present diffraction peaks in the powder pattern illustrate high crystallinity of the products of wurtzite-type ZnO structure (ICDD PDF No. 80-0074), space group $P6_3mc$ (186). No diffraction peaks belonging to any other compound are found, demonstrating the high purity of the obtained product. Due to the broadening of diffraction peaks, the overlapping of neighboring peaks can be observed such as the overlapping of (200), (112) and (201). The volume-weighted average crystallite size calculated from the Rietveld profile refinement is 6.9 nm. The other structural parameters obtained from Rietveld profile refinement such as unit cell parameters, fractional atomic coordinates, and microstrain are listed in Table S1.

The morphology and the size distribution of as prepared powder were further examined with transmission electron microscopy (TEM) as shown in Fig. 2. From Fig. 2(a), one can observe that the particles with small agglomerates have rather uniform near-sphere shape as well as size. The clear lattice fringes displayed in Fig. 2(b) demonstrate the high crystallinity and random orientation of the ZnO nanoparticles. A high-resolution TEM image of an isolated ZnO nanocrystal is also shown in Fig. 2(c). The interplanar spacing is estimated to 0.282 nm which corresponds to (100) lattice plane of ZnO, and the size of such a well-defined particle can be easily measured to be 8.7 nm. Furthermore, the size distribution curve of nanoparticles was obtained by measuring several hundred nanocrystals from HRTEM images and shown in Fig. 2(d). The statistic result, 8.4 ± 1.3 nm, has a good agreement with the result of XRD. Both of them demonstrate that the as-synthesized ZnO nanoparticles do have a small grain size. And the specific surface area estimated from BET method is 81.0 $m^2/g$.

In general, ZnO is very easy to crystallize even in pretty facile situation. For instance, 90 ºC and 1.5 h are enough to obtain micron-sized ZnO crystals from the mixing aqueous solution of $Zn(NO_3)_2$ and hexamethylenetetramine.[26,27] Moreover, high agglomerations are always observed in nanocrystals owing to the high surface energy which is the nature of nanomaterials.[28] When smaller the particle size is, more serious agglomeration occurs. However, the ZnO nanoparticles prepared under solvothermal conditions at 100 ºC for 4 h in this work, not only have small grain size but also have slight agglomerations. These are attributed to the use of methanol which acts as both solvent and crystal growth inhibitor instead of water and other alcohols. The formation process of the slight-agglomeration nanoscaled ZnO nanocrystalline particles is schematically illustrated in Fig. 3. At the beginning, zinc acetate and potassium hydroxide ionize $Zn^{2+}$ and $OH^-$ in the corresponding solution. Once the solution of potassium hydroxide was added to zinc acetate solution, the ionized $Zn^{2+}$ and $OH^-$ will react to form $Zn(OH)_2$. The formation of ZnO crystal nuclei from the formed $Zn(OH)_2$ is a complicated process, but it mainly relies on the dehydration of hydroxyl belonging to $Zn(OH)_2$.[29,30] At the surface of ZnO crystal nuclei, the bonding hydroxide ions form hydrogen bonds with methanol, and the methyl which shows positive electricity points to the solvent. Such a positively charged surface will repel the other equally positively charged nuclei. And the methyl is stable with $Zn(OH)_2$, which acts as an inhibitor to limit the growth of ZnO nuclei. Those mean that methanol used as solvent in this work also acts as an inhibitor to limit the growth and agglomeration of ZnO, and further leading to slight-agglomeration nanoscaled ZnO. Generally, water and some other longer carbon link alcohols are used as solvent for ZnO preparation. Owing to the similar structure, all of them can form hydrogen bond with the capped ZnO nuclei, but the tiny differences in structure between them and methanol make water and other long C link alcohols less suitable in inhibiting the growth and agglomeration of ZnO particles. Water molecule has a stronger hydrogen bond with the hydroxyl bonding to the surface of ZnO nuclei than methanol, but $H_2O$ is easy to ionize hydroxyl and proton. The ionization of $H_2O$ will cause the opposite charge of the nuclei and proton transfer between ZnO nuclei. As for other longer C link alcohols, the longer C link weakens the hydrogen bond, which results in a weaker inhibition. These make methanol the most suitable agent to as-synthesized ZnO nanoparticles with slight agglomerations as solvent. We recently reported that the size of ZnO quantum dots can be tuned by different alcohols.[31] To be more specific, the sizes of ZnO quantum dots prepared using methanol, ethanol and hexanol under similar experimental conditions are 3.3, 5.6 and 7.8 nm, respectively. This finding can be explained by the above highlighted growth mechanism and thus making it reasonable.

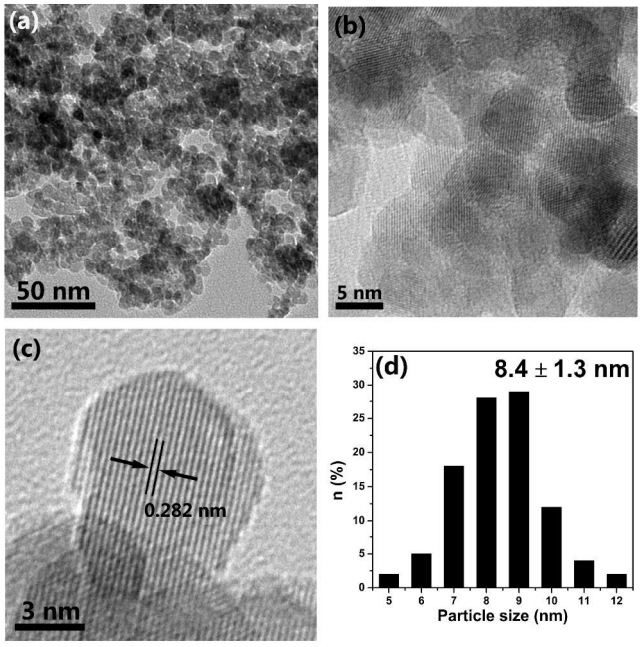


**Fig. 2** TEM image (a), HRTEM image (b) of ZnO nanoparticles, HRTEM image of an isolated ZnO nanoparticle (c), and size distribution of ZnO nanoparticles by measuring the size of more than one hundred ZnO nanoparticles from HRTEM images (d).

To evaluate the potential applicability in gas sensor for n-butanol gas, we investigated fundamental gas sensing properties of the as-synthesized ZnO nanoparticles. The sensing performances of a sensor not only depend on the gas atmosphere but also on the operating temperature. To be more specific, there exists a range of temperature for the sensor to

show the highest gas response under the same other conditions.[19,25] Fig. S3 shows the variation of resistance with temperature, and a typical negative temperature coefficient of resistance can be found. Fig. S4 shows the temperature dependence of gas response for investigated sensor. One can find that 320 ºC is the optimal operating temperature for as-fabricated ZnO nanocrystalline powder gas sensor. Fig. 4(a) displays the dynamic response to different n-butanol concentration from 10 to 1000 ppm in dry air at an operating temperature of 320 ºC. Before n-butanol gas is injected, the gas response keeps 1 without big fluctuation. Once the gas is injected, the gas response increases fast and reaches almost its constant. When the sensor is exposed to air ambient again, the response value decreases rapidly to the baseline. And one can also find that the sensor based on ZnO nanoparticles has a good response to the n-butanol gas. It can detect a concentration as low as 10 ppm toward which the gas response is 4.3. Its gas response to 100, 300, 500, 700 and 1000 ppm n-butanol gas is 62, 368, 805, 1237 and 1988, respectively. As we have announced in the introduction, the maximum acceptable concentration of n-butanol in working shops is stipulated as 152-303 mg/m$^3$ which corresponds to 45-90 ppm, and the lower explosive limit is 1.45% by volume which corresponds to 14500 ppm. Hence, the fabricated gas sensor based on ZnO nanoparticles is extremely sensitive toward n-butanol gas, and its gas response is well satisfied with the detection needs of n-butanol in aspects of noxious and inflammable gas.

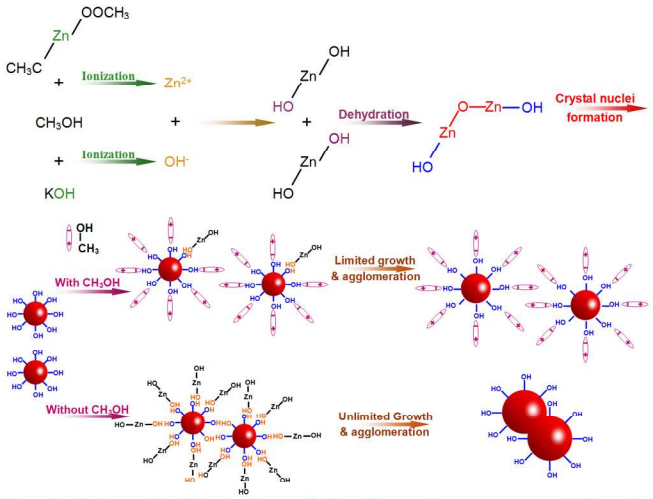


**Fig. 3** Schematic illustration of the formation process of the ZnO nanoparticles.

The gas response to n-butanol at operating temperature of 320 ºC also shows a good linear dependence on the gas concentration. As shown in Fig. 4(b), the line for n-butanol is the calibration curve and the experimental data were fitted as:

$$\beta = 2.077\,C - 171.282 \qquad (1)$$

and the low detection limit is calculated to 82.95 ppm according to this equation, but the sensor can easily detect as low as 10 ppm (Fig. 4(a)). It means that equation 1 is not suitable for the low concentration. Hence, another equation based on the experimental data (Fig. 4(a)) obtained at concentrations lower than 100 ppm was fitted as:

$$\beta = 0.382C + 0.458 \qquad (2).$$

According to this equation, the low detection can be estimated to be 1.42 ppm which is much more convincible. Noticing that, the dependence between gas response and concentration is described by a piecewise function which is made up of equation 1 and 2. The equation 2 is suitable for low concentration while the equation 1 suits high concentration. The reasons why there exist two different equations in different concentration range need further investigations.

At the same time, the response to other common VOCs such as ethanol, acetone and isopropanol in different concentrations from 50 to 1500 ppm were also measured at 320 ºC respectively. The dynamic response-recovery curves are shown in Fig. S5 and summarized in Fig. 4(b). According to the corresponding fitted curves displayed in the same figure, all of them exhibit a good linear relationship. Compared with the gas response to n-butanol at the same concentration, the others are much lower. More specifically, the gas response to n-butanol is roughly 5.6, 10.6 and 10.0 times higher than that to ethanol, acetone and isopropanol gases at the concentration of 1000 ppm, respectively. It means the gas sensor based ZnO nanoparticles has a good selectivity to n-butanol among the examined VOCs gases.

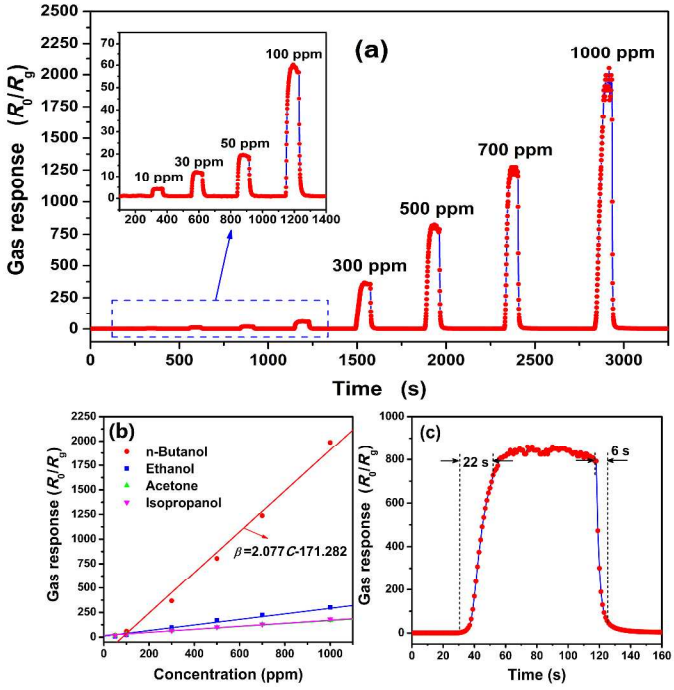


**Fig. 4** Dynamic response to different n-butanol concentration from 10 to 1000 ppm in dry air (a), variation of sensor response to different concentrations of target gases (b), and dynamic response to 500 ppm n-butanol gas in dry air (c) at an operating temperature of 320 ºC.

The response and recovery time are also very important parameters for gas sensor. In Fig. 4(c), a magnifying dynamic response to 500 ppm n-butanol gas in dry air at an operating temperature of 320 ºC is exhibited. Based on the definition of response and recovery time, they are calculated to 22 and 6 seconds, respectively. Both of them illustrate a fast response and recovery properties toward n-butanol gas of as-fabricated sensor. Moreover, the repeatability of as-fabricated gas sensor is also investigated by testing 500 ppm n-butanol for five times at the same conditions and shown in Fig. 5. It shows that all of the gas responses can reach 800 with only small fluctuation. To be more specific, the error limit is only 4.2%. And the response as well as recovery time do not have much difference. So, the sensor based on ZnO nanoparticles shows a good repeatability. Not only that, the stability of the gas sensor is also verified by

testing the gas response toward 500 ppm n-butanol in 25 days. The gas response evolution is shown in Fig 6, and one can find that the response only has a small fluctuation which is below 7.3% of its initial value. It illustrates a good stability of the gas sensor.

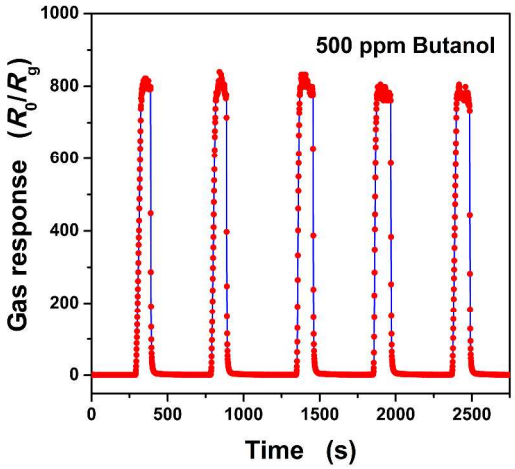


**Fig. 5** Dynamic response-recovery cycles of as-fabricated gas sensor toward 500 ppm n-butanol gas at an operating temperature of 320 ºC.

Table 1 compares the sensing performance of as-prepared ZnO nanoparticles against previously reported metal oxide semiconductor-based sensor toward n-butanol gas. The extremely high response which is 630 at 150 ºC for 10 ppm n-butanol gas was reported for mesoporous $SnO_2$ prepared with hydrothermal treatment.[3] However the recovery time is poor, and it is hard for the sensor to recover to the initial state after exposing to the air until an additional heating treatment at 300 ºC is used. Even with the heating treatment, it still needs more than 120 s to return the initial work state, which is not satisfied with the need of real time monitor. Apart from the mesoporous $SnO_2$ reported by Wang,[3] the as-fabricated sensor has a highest sensitivity. Moreover, most reported sensors reach their saturation in a concentration lower than 500 ppm,[15,16,18,19,23] and the sensors are hard to reflect concentration which is higher than their saturation concentration. But the sensor in this work shows a pretty good linear relationship in a wide range from 10 ppm to 1000 ppm even higher.

The principle of n-butanol detection of the as-fabricated sensor is based on its conductance variation, which can be interpreted by Wolkentein's model,[32,33] as shown in Fig.7. Oxygen species in the air are adsorbed on the ZnO particle surface and ionized to adsorbed oxygen ions ($O^-_{ads}$ and $O^{2-}_{ads}$) by capturing free electrons from the particles, which leads to the formation of a thick space-charge layer and a consequent a high resistance of the sensor. This process can be described using the following equations:

$$O_{2gas} \leftrightarrow O_{2ads} \quad (3)$$

$$O_{2ads} + e^- \leftrightarrow O^-_{2ads} \quad (4)$$

$$O^-_{2ads} + e^- \leftrightarrow 2O^-_{ads} \quad (5)$$

$$O^-_{ads} + e^- \leftrightarrow O^{2-}_{ads} \quad (6)$$

When the sensor was exposed to n-butanol gas, n-butanol would react with $O^-_{ads}$ or $O^{2-}_{ads}$ to form $CO_2$ and $H_2O$. And the electrons captured by $O^-_{ads}$ or $O^{2-}_{ads}$ would be released again, which results in thinning of space-charge layer and decreasing of potential barrier. This process leads to decrease of resistance and can be expressed as follows:[18,23]

$$(C_4H_9OH)_{gas} \leftrightarrow (C_4H_9OH)_{ads} \quad (7)$$

$$(C_4H_9OH)_{ads} + 12O^{2-}_{ads} \rightarrow 4CO_2 + 5H_2O + 24e^- \quad (8)$$

$$(C_4H_9OH)_{ads} + 12O^-_{ads} \rightarrow 4CO_2 + 5H_2O + 12e^- \quad (9)$$

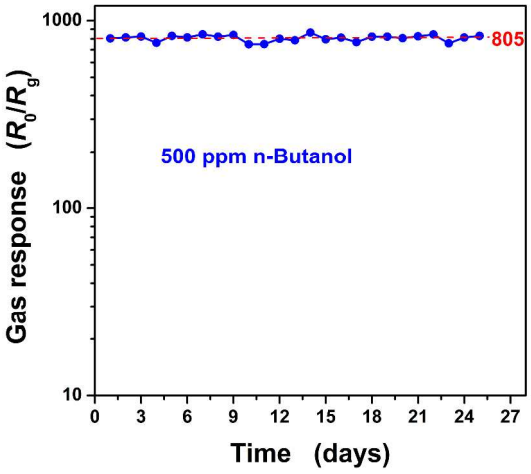


**Fig. 6** Dynamic response-recovery cycles of as-fabricated gas sensor toward 500 ppm n-butanol gas at an operating temperature of 320 ºC.

According to the analysis of the possible gas sensing mechanism, one can find that $O^-_{ads}$ and $O^{2-}_{ads}$ have a great influence on gas sensing properties of the ZnO nanoparticles. And the existence of formed adsorbed oxygen ions can be easily detected by X-ray photoelectron spectroscopy (XPS). Hence, XPS was carried out, and the results were shown in Fig. S6. From Fig. S6(a), Zn2p spectra reveal two peaks of $Zn2p_{3/2}$ and $Zn2p_{1/2}$ at 1021.4 eV and 1044.4 eV with a good symmetry indicate that Zn in the particles is in a single form of $Zn^{2+}$. The splitting of the 2p doublet is 23.0 eV which is in good agreement with the energy splitting reported for ZnO and corresponding to a 2p binding energy of Zn(II) (indexed Standard ESCA Spectra of the Elements and line Energy Information, *Φ* Co., USA).[34] Fig. S6(b) shows O1s XPS spectra, where one can find that there are two components of oxygen varying in chemical states with $O_{latt}$ (530.16 eV) and $O^-_x$ (531.70 eV). $O_{latt}$ is attributed to oxygen ions in the crystal lattice which is thought to be pretty stable and have no contribution to the gas response. On the other hand, $O^-_x$ is the adsorbed oxygen ion which is mainly discussed in gas sensing mechanism section in the oxygen deficient regions such as oxygen vacancy ($V_O$), oxygen interstitial ($O_i$), and oxygen antisite ($O_{Zn}$).[11] To some degree, the peak area ratio of $O^-_x$ and $O_{latt}$ can represent the related concentrations of these two kinds of oxygen chemical states. In this work, that ratio of as-prepared ZnO nanoparticles is calculated to be 0.66 which means a high concentration of $O^-_x$ in as-prepared ZnO nanoparticles.

**Table 1** Comparison of the sensing performances of various semiconductor metal oxide based gas sensor toward n-butanol.

| Materials | Concentration (ppm) | Operating temperature (°C) | Sensitivity | References |
|---|---|---|---|---|
| Mesoporous $SnO_2$ | 10 | 150 | 630 | 3 |
| ZnO nanoflakes | 500 | 330 | 87 | 14 |
| Au/ZnO nanowires | 400 | 320 | 28 | 15 |
| ZnO microflowers | 100 | 320 | 24.1 | 16 |
| ZnO/α-$Fe_2O_3$ nanorods | 100 | 225 | 57 | 18 |
| $SnO_2$ nanospheres | 100 | 120 | 32.3 | 19 |
| α-$Fe_2O_3$ hollow spindles | 100 | 280 | 13.9 | 20 |
| $ZnSnO_3$ cubes | 100 | 300 | 9 | 21 |
| NiO hollow microspheres | 500 | 350 | 2.5 | 23 |
| ZnO nanoparticles | 100<br>500 | 320 | 62<br>805 | This work |

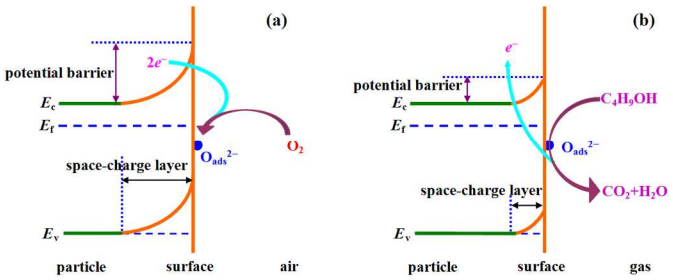


**Fig. 7** A schematic diagram of the proposed reaction mechanism of ZnO based sensor to n-butanol in air (a) and in n-butanol (b), respectively.

The high response, fast response/recovery of as-fabricated sensor toward n-butanol gas is thought to be attributed to the high specific surface area (81.0 $m^2/g$) and the high concentration of $O_x^-$. As we have introduced, the gas sensing property of semiconductor metal oxide is based on the reactions between gases and $O_x^-$ belonging to sensing materials. A higher specific surface area brings to more contact area between gases and the metal oxide, which not only benefits to a fast gas diffusion leading to a quick response and recovery but also is helpful for having more $O_x^-$ exposed to react with gases. According to the chemical reaction kinetics, a higher reactant ($O_x^-$) concentration will naturally cause a faster reaction rate and higher reaction extent. At the same time, the high specific surface area and high concentration of $O_x^-$ should be responsible for the higher sensitivity of as-prepared ZnO nanoparticles than that of the other nanostructure listed in Table 1. However, good selectivity and piecewise linear relationship between response and concentration need further investigations.

## 4. Conclusions

ZnO nanoparticles were successfully synthesized by a simple low-temperature solvothermal method. The wurtzite-type and highly crystalline ZnO nanoparticles with particle size of 8.4 nm with uniform near-sphere shape and high specific surfacearea were obtained. Such small particle size and slight agglomeration are attributed to the use of methanol which acts both as solvent and inhibitor of growth and agglomeration. The obtained ZnO nanoparticles were used directly to fabricate gas sensor device which shows a high-performance gas sensing properties including high sensitivity, good selectivity, fast response /recovery time, good repeatability and stability toward n-butanol gas. The high performance is attributed to its high specific surface area and high concentration of $O_x^-$, which resulted from the small grain size. Such a sensor based on ZnO nanoparticles is very promising for the practical detector design for n-butanol gas.

## Acknowledgements

This work was supported by the National Natural Science Foundation of China (Grant No.51262029), the Key Project of the Department of Education of Yunnan Province (ZD2013006), Program for Excellent Young Talents, Yunnan University (XT412003), Department of Science and Technology of Yunnan Province via the Key Project for the Science and Technology (Grant No.2011FA001), and National Training Program of Innovation and Entrepreneurship for Undergraduates (No. 201310673026). Igor Djerdj acknowledges financial support from the Unity through Knowledge Fund (www.ukf.hr) of the Croatian Ministry of Science, Education and Sports (Grant Agreement No. 7/13), and from the Croatian Center of Excellence for Advanced Materials and Sensing Devices.

## Notes and references

[a]School of Physics Science and Technology, Yunnan University, 650091 Kunming, People's Republic of China.
[b]Yunnan Province Key Lab of Micro-Nano Materials and Technology, Yunnan University, 650091 Kunming, People's Republic of China. Fax: +8687165153832; Tel: +8687165031124; E-mail: ydwang@ynu.edu.cn.
[c]Ruđer Bošković Institute, Bijenička 54, 10000 Zagreb, Croatia. Fax: +38514680114; Tel: +38514680113; E-mail: igor.djerdj@irb.hr.

Electronic Supplementary Information (ESI) available: [Table S1. Structural and microstructural parameters extracted from the Rietveld refinement of powder XRD pattern; Fig. S1 Cross section and surface SEM images of the sensors; Fig. S2. (a) A photograph of the WS-30 A testing system, (b) the basic testing principle, (c) the schematic structure of the gas sensor, and (d) the picture of a completed gas sensor; Fig. S3 Variation of resistance with temperature; Fig. S4. Gas response of as-fabricated gas sensor toward 500 ppm n-butanol gas tested at different

temperatures; Fig. S5. Dynamic response curves of as-fabricated sensor toward ethanol, acetone and isopropanol at 320 ºC; Fig. S6. The high-resolution XPS spectra of (a) Zn2p and (b) O1s of ZnO nanoparticles.]. See DOI: 10.1039/b000000x/

1. M. R. R. Khan, B. H. Kang, S. H. Yeom, D. H. Kwon and S. W. Kang, *Sens. Actuators, B*, 2013, **188**, 689.
2. H. Nguyen and S. A. El-Safty, *J. Phys. Chem. C*, 2011, **115**, 8466.
3. H. Wang, Y. Qu, H. Chen, Z. D. Lin and K. Dai, *Sens. Actuators, B*, 2014, **201**, 153.
4. A. B. Djurišić and Y. H. Leung, *Small*, 2006, **2**, 944.
5. H. Hagendorfer, K. Lienau, S. Nishiwaki, C. M. Fella, L. Kranz, A. R. Uhl, D. Jaeger, L. Luo, C. Gretener, S. Buecheler, Y. E. Romanyuk and A. N. Tiwari, *Adv. Mater.*, 2014, **26**, 632.
6. T. Meron and G. Markovich, *J. Phys. Chem. B*, 2005, **109**, 20232.
7. Y. Z. Jin, J. P. Wang, B. Q. Sun, J. C. Blakesley and N. C. Greenham, *Nano Lett.*, 2008, **8**, 1649.
8. N. Satio, H. Haneda, T. Sekiguchi, N. Ohashi, I. Sakaguchi and K. Koumoto, *Adv. Mater.*, 2002, **14**, 418.
9. M. H. Huang, S. Mao, H. Feick, H. Yan, Y. Wu, H. Kind, E. Weber, R. Russo and P. Yang, *Science*, 2001, **292**, 1897.
10. S. J. Pearton, D. P. Norton, K. Ip, Y. W. Heo and T. Steiner, *Prog. Mater. Sci*., 2005, **50**, 293.
11. X. Y. Cai, D. Hu, S. J. Deng, B. Q. Han, Y. Wang, J. M. Wu and Y. D. Wang, *Sens. Actuators, B*, 2014, **198**, 402.
12. J. Zhang, S. Wang, M. J. Xu, Y. Wang, B. Zhu, S. Zhang, W. Huang and S. Wu, *Cryst. Growth. Des*., 2009, **9**, 3532.
13. C. Dong, X. Liu, X. Xiao, G. Chen, Y. Wang and I. Djerdj, *J. Mater. Chem. A*, 2014, **2**, 20089.
14. Y. V. Kaneti, J. Yue, X. Jiang and A. Yu, *J. Phys. Chem. C*, 2013, **117**, 13153.
15. C. Gu, L. Shanshan, J. Huang, C. Shi and J. Liu, *Sens. Actuators, B*, 2013, **177**, 453.
16. J. Huang, Y. Wu, C. Gu, M. Zhai, K. Yu, M. Yang and J. Liu, *Sens. Actuators, B*, 2010, **146**, 206.
17. L. Wang, S. Wang, H. Zhang, Y. Wang, J. Yang and W. Huang, *New J. Chem.*, 2014, **38**, 2530.
18. Y. V. Kaneti, Q. M. D. Zakaria, Z. Zhang, C. Chen, J. Yue, M. Liu, X. Jiang and A. Yu, *J. Mater. Chem. A*, 2014, **2**, 13283.
19. H. Zhang, Q. He, X. Zhu, D. Pan, X. Deng and Z. Jiao, *CrystEngComm*, 2012, **14**, 3169.
20. J. Huang, M. Yang, C. Gu, M. Zhai, Y. Sun and J. Liu, *Mater. Res. Bull.*, 2011, **46**, 1211.
21. J. Huang, X. Xu, C. Gu, W. Wang, B. Geng, Y. Sun and J. Liu, *Sens. Actuators, B*, 2012, **171-172**, 572.
22. J. Huang, X. Xu, C. Gu, M. Yang, M. Yang and J. Liu, *J. Mater. Chem.*, 2011, **21**, 13283.
23. G. Zhu, C. Xi, H. Xu, D. Zheng, Y. Liu, X. Xu and X. Shen, *RSC Advances*, 2012, **2**, 4236.
24. J. Xu, Q. Pan, Y. Shun and Z. Tian, *Sens. Actuators, B*, 2000, **66**, 277.
25. Y.D. Wang, I. Djerdj, M. Antonietti and B. Smarsly, *Small*, 2008, **4**, 1656.
26. L. E. Greene, B. D. Yuhas, M. Law, D. Zitoun and P. Yang, *Inorg. Chem.*, 2006, **45**, 7535.
27. L. E. Greene, M. Law, J. Goldberger, F. Kim, J. C. Johnson, Y. Zhuang, R. J. Saykally and P. Yang, *Angew. Chem. Int. Ed.*, 2003, **42**, 3031.
28. L. R. Singh, R. S. Ningthoujam and S. D. Singh, *J. Alloy. Compd.*, 2009, **487**, 466.
29. A. Kawska, P. Duchstein, O. Hochrein and D. Zahn, *Nano Lett.*, 2008, **8**, 2336.
30. S. Xu and Z. L. Wang, *Nano Res.*, 2011, **4**, 1013.
31. X. Liu, X. X. Xing, Y. X. Li, N. Chen, I. Djerdj and Y. D. Wang, *New J. Chem.*, 2015, DOI: 10. 1039/c5nj00070j.
32. T. Wolkenstein, Electronic Processes on Semiconductor Surface during Chemisorption (New York: Consultants Bureau), 1991, 35.
33. T. Chen, Q. J. Liu, Z. L. Zhou and Y. D. Wang, *Nanotechnology*, 2008, **19**, 095506.
34. C. D. Wagner, W. M. Riggs, L. E. Davis, J. F. Moulder, G. E. Muilenberg, Handbook of X-ray Photoelectron Spectroscopy, PerkinElmer, Prairie, 1979, 80.

Solvothermally synthesized ZnO nanoparticles applied as a sensing layer for n-butanol gas sensor show a very good gas response performance.